Nanoscale Advances

Accepted Manuscript

This article can be cited before page numbers have been issued, to do this please use: P. Sahariya, A. Murali, S. Mohan, A. Lakshminarayanan, S. Sekar, D. M, R. Redrouthu and S. S. Han, *Nanoscale Adv.*, 2023, DOI: 10.1039/D3NA00644A.

ROYAL SOCIETY OF CHEMISTRY

rsc.li/nanoscale-advances

ROYAL SOCIETY OF CHEMISTRY
View Article Online
DOI: 10.1039/D3NA00644A

Nanoscale Advances

PAPER

In-vitro anti-prostate adenocarcinoma and lung cancer studies of phenoxyaniline blocked poly(methyl methacrylate) based nanocomposites *via* controlled radical polymerization

Received 00th January 20xx,
Accepted 00th January 20xx

DOI: 10.1039/x0xx00000x

www.rsc.org/

Sahariya Priya,[a] Adhigan Murali,[b,*] Sakar Mohan,[c] A. Lakshminarayanan,[d] S. Sekar,[b] R. Ramesh,[e,*] M. Devendiran,[f] Sung Soo Han,[a,*]

Phenoxyaniline-based macroinitiator is utilized for the first time in order to produce phenoxyaniline-*blocked*-poly(methyl methacrylate) composites through single electron transfer-living radical polymerization (SET-LRP) under mild conditions. A different weight percentage of Cloisite 93-A is added into the polymer mixtures in order to increase their biochemical properties. The prepared blocked copolymer nanocomposites are characterized using ATR-IR, UV-*vis*-spectroscopy, XRD, Raman, TGA, DSC, Particle size analyzer, contact angle measurement and SEM in order to characterize their structural, thermal, surface and morphological properties. Further, the developed polymeric nanocomposites are successfully applied in two different cancer cell lines (prostate adenocarcinoma and lung cancer), which show excellent anticancer properties. Also, the acridine orange/ ethidium bromide (AO\EtBr) dual staining is performed, which caused a drastic cell death by apoptosis in both A549 and PC-3 cell lines, which indicated that the prepared polymeric nanocomposites effectively inhibit the cell proliferation and induce the apoptosis in both the cancer cells. Here the nanoclay is used for cancer treatment because of their complete water soluble in nature, which essentially forms a cationic complex between the clay and drug through electrostatic interactions. Hence, the exchange of ions between the clay and other ions in the biological environment is led to inhibit the proliferations of the prostate adenocarcinoma and lung cancer cells in the system.

1 Introduction

Till date, chemotherapy is one of the major techniques to treat many cancers. However, during the chemotherapy treatment, some of the healthy cells can also be destroyed and lead to serious side effects. In order to address this issue in the chemotherapy treatments of various tumour cells, some of the alternative cancer treatments have been emerged, which include the targeted drug delivery systems as one among them.[1] Nano-based drugs or medicines are playing a major role in this field by contributing many advantages over drug delivery methods, diagnosis, enhanced cancer imaging and targeting of particular cancer cells, etc. Moreover, nano-based drugs can enhance active or passive cancer targeting and thus increase the selectivity, lower the toxicity and prolong the half-life span in the human body. Also, surface-charge of nanoparticles (such as clay particles) plays an important role on their interaction with cell surface for the effective cellular up-take.[2] Derivatizing and existing new drug is a significant approach for the development of new anticancer agent.

In this direction, Yogesh et. al., reported a azo-schiff base ligands like 2-((E)-((4-(diethylamino)phenyl)imino)methyl)-4-((E)-(2 phenylamino)phenyl)diazinyl)phenol containing Zn(II) complexes, which have been analyzed for their effective cytotoxicity properties against Hut-78 cell line.[3] Hosseini et.al, also reported a doxorubicin-based bentonite nanoclay complex and used to treat the melanoma cells, which showed effective targeted drug delivery properties.[4] Generally, nanoparticulate clay, which we used in anti-cancer treatment, has drawn a great attention as a drug carrier due to their better bio-compatibility, high specific surface area and high

[a]*School of Chemical Engineering, Yeungnam University, 280 Daehak-Ro, Gyeongsan, Gyeongbuk 38541, Republic of Korea*
[b]*School for Advanced Research in Petrochemicals (SARP)- ARSTPS, Central Institute of Petrochemicals Engineering & Technology (CIPET), Govt. of India, Chennai-600032*
[c]*Centre for Nano and Material Sciences, Jain University, Bangalore 562112, Karnataka, India.*
[d]*Department of Pharmacology, Indira Medical College and Hospitals, Tiruvallur, Tamilnadu, 631 203*
[e]*Department of Chemical Engineering, School of Mechanical, Chemical and Material Engineering, Adama Science and Technology University, Adama, P.O. Box: 1888, Adama, Ethiopia*
[f]*Vels Institute of Science Technology and Advanced Studies (VISTAS), Pallavaram, Chennai -117, India*
**E-mail: precymurali@gmail.com (AM); ramesh.redrouthu@astu.edu.et (RR); sshan@yu.ac.kr (SSH)*

adsorption behavior. For example, aluminosilicate-based nanoclay acts as an excellent drug delivery carrier in cancer cell lines towards particular tumour sites.[5] On the other hand, the most frequently used acrylic derivatives polymers such as polymethyl methacrylate, polymethacrylic acid and acrylamide for the effective controlled-release of drugs in active tumour cells.[6,7] Krishna et.al, reported the acrylic derivative-based PMMA microgels for the controlled release of an anti-cancer treatment, which suggested that the ionic transport was controlled more by relaxation of poly(methacrylic acid) gel due to presence of ionization of carboxylic groups through electrostatic repulsion between adjacent ionized groups.[8] Seyedeh et. al., also reported PMMA coated chitosan-glutathione conjugates, which have been analyzed for their anticancer activities against NIH 3T3, T47D breast carcinoma cells and HT29, CaO_2 colon cell lines.[9] Several researchers have made attempted to synthesize various co-polymer materials (di-block or triblock) for anticancer treatments thanks to their sensitivity, selectivity, compatibility and low cytotoxicity with different cancer cell lines. In this way, Caner et. al., reported paclitaxel-based drug loaded amphiphilic star hyperbranched block copolymer for targeted anti-cancer applications.[10] In this direction, herein, we have utilized the above characteristic behavior of copolymer in cancer cells and to our best of knowledge, this is the first time that the phenoxyaniline blocked PMMA through single electron transfer-living radical polymerization has been introduced for anticancer treatments against the prostate adenocarcinoma and lung cancer cell lines.

2. Experimental

2.1 Materials

Methyl methacrylate (MMA: $C_5H_8O_2$, Mw: 100.12 g/mol, and 99% purity) monomer, 3-phenoxyaniline ($C_{12}H_{11}NO$, Mw: 185.22 g/mol, and 98% purity) was procured from Sigma-Aldrich, USA and the monomer further purified by passing it through an alumina column (removal of inhibitor) before use. Bromoisobutyryl, bromide [$(CH_3)_2CBrCOBr$], N, N, N^{I}, N^{II}, N^{III}-Pentamethyldiethylenetriamine [PMDETA, $[(CH_3)_2NCH_2CH_2]_2NCH_3)$], and copper (0) powder, 99.9% were received from Sigma-Aldrich, USA and used as received. Cloisite 93A (particle size <2 µm) was obtained from Rock wood Additives. Organic solvents (dimethyl sulfoxide (DMSO), triethylamine (Et_3N), dimethyl formamide (DMF), tetrahydrofuran (THF), and hexane were dried and distilled before use. Lung cancer cell lines (A549) and human prostate cancer cell lines (PC-3) were purchased from National Centre for Cell Science (NCCS), Pune, India. Cell proliferation kit I (MTT) assay, acridine orange (AO), ethidium bromide (EtBr) and phosphate buffer saline (PBS) was procured from Sigma-Aldrich, USA.

2.2 Characterization methods

Raman spectra were recorded on a confocal Raman spectrometer (Alpha 300R, WITec GmbH, Germany, Excited at 532 nm using laser of Ne). FT-IR of polymeric materials were analyzed using Thermo scientific-NICOLET 6700 model under transmittance mode. The scanning electron microscopy (SEM) from JEOL, JSM-IT800 with super hybrid lens operated at 30 kV was used to afford the images. The particle size distribution analyses were performed on a Litesizer 500 model from Anton Paar, USA. Thermal analysis was executed by DSC Q-200 and TGA Q-50, TA instruments (WATERS), Astria. Molecular weight distribution was determined by gel permeable chromatography (GPC) from Shimadzu, Japan. UV-vis absorption spectra were recorded on Elico SL-159 spectrometer and X-ray diffraction (XRD) using Cu Kα=1.54060 Å from Rigaku, Japan. Surface wettability of coated film was measured using water contact angle (Halmarc HO-IAD-Cam-O1B). Micro ELISA plate reader and flow cytometer was used and cells were washed two times before analysis of fluorescence intensity, further stained and viewed under fluorescence microscope at 20x magnification.

2.3 Cell viability (MTT) assay

The cell viability of DST-28 (phenoxyanilne-b-PMMA with nanoclay) treated PC-3 cells was assessed by MTT assay. The assay is based on the reduction of soluble yellow tetrazolium salt to insoluble purple formazan crystals by metabolically active cells. PC-3 cells were plated in 48 well plates at a concentration of $2x10^4$ cells/well 24 hours after plating, cells were washed twice with 500 µL of serum-free medium and starved by incubating the cells in serum-free medium for 3 hours at 37°C. After starvation, cells were treated with DST-28 at different concentrations (10-120 µg/mL) for 24 hours. At the end of treatment, the medium from control and DST-28 treated cells were discarded and 200 µL of MTT containing DMEM (0.5 mg/ml) was added to each well. The cells were then incubated for 4 h at 37ºC in the CO_2 incubator. The MTT containing medium was then discarded and the cells were washed with 1x PBS. The crystals were then dissolved by adding 200 µL of solubilization solution and this was mixed properly by pipetting up and down. Then the formazan crystals formed were dissolved in dimethyl sulfoxide (200 µL) and incubated in dark for an hour. Then the intensity of the color developed was assayed using a Micro ELISA plate reader at 570 nm. The number of viable cells was expressed as a percentage of control cells cultured in a serum-free medium. Cell viability in the control medium with-out any treatment was represented as 100%. The cell viability is calculated using the formula: % cell viability = [570 nm of treated cells/570 nm of control cells] × 100. Based on the MTT assay, we selected the optimal doses (IC-50: 40 µg/mL) for further studies. Analysis of cell morphology changes by a phase-contrast microscope. $3×10^4$ cells were seeded in 6 well plates and treated with DST-28 (40 µg/mL for PC-3 cells) for 24h. At the end of the incubation period, the medium was removed and cells were washed once with a phosphate buffer saline (PBS pH 7.4). The plates were observed under a phase-contrast microscope. Cell viability of DST-24 treated A-549 lung cancer cell lines was assessed using MTT assay. The assay was based on reducing the soluble yellow tetrazolium salt to insoluble purple formazan crystals by metabolically active cells. In this study, the A-549 cells were plated in 48 well plates ($2x10^4$ cells/well). After 24 h, cells were

washed twice with 500 µL serum free medium and starved for 3 h at 37 °C. Then, the cells were treated with DST-24 (25-150 µg/mL) for 24 h. After treatment, control and treated cells media were discarded. The MTT (200µL, 0.5 mg/mL in DMEM) was added, incubated for 4 h at 37 °C, and then discarded. Cells were washed with 1xPBS. The crystals were dissolved using 200 µL solubilization solution, mixed and then dissolved in DMSO (200 µL). Intensity was measured at 570 nm using a Micro ELISA plate reader. Viable cells were expressed as percentage of control in serum-free medium (100%) for untreated control. Optimal doses (IC-50: 50 µg/mL) were selected based on MTT assay. The change in cell morphology was analyzed using phase-contrast microscope. Around $3x10^4$ cells seeded in 6-well plated, treated with DST-24 (50 µg/mL) for A-549 cells for 24 h. After incubation, the medium was removed, and cells were washed with PBS (pH 7.4).

2.4 Determination of mode of cell death by acridine orange (AO)/ethidium bromide (EtBr) dual staining

The effects of DST 28 in PC-3 cell death were also determined by AO/EtBr dual staining as described previously.[11] The cells were treated with DST-28 for 24 h and then the cells were harvested, washed with ice-cold PBS. The pellets were resuspended in 5 µL of acridine orange (1 mg/mL) and 5 µL of EtBr (1 mg/mL). The apoptotic changes of the stained cells were then observed by using a fluorescence microscope.

2.5 Synthesis of phenoxyaniline (PA) based macroinitiator

0.37 g of 3-phenoxyaniline was dissolved in 15 mL of DCM, further transferred into 50 mL of round-bottom flask and kept in ice bath. After, 30 min., 0.54 mL (2 mM) of trimethylamine was added in the above mixture and stirred for another 30 min at 0 °C. Ice cubes were added into ice bath to bring the temperature to 0 °C. After, that 0.48 mL (2 mM) of α-bromoisobutrylbromide was added drop by drop using glass syringe and stirred for 24 h at 0 °C under N_2 atmosphere (see Scheme 1). Finally, 20 mL of diethylether was used to terminate the reaction and further obtain white color crystals (PA-initiator).

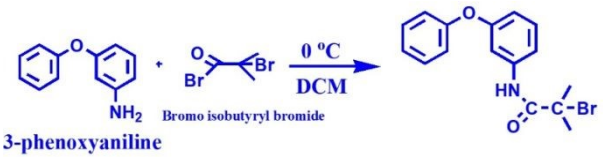

Scheme 1. Synthesis of phenoxyaniline based macroinitiator.

2.6. Preparation of phenoxyaniline-b-PMMA through SET-LRP method

0.25 g of 3-phenoxyaniline-based initiator was dissolved in 5 mL of tetrahydrofuran (THF) and 2 mg of degassed Cu(0) powder was added into the above mixture. The mixture was transferred into 50 mL of round bottom flask. Further, Deoxygenated MMA (4.0 mL) was added to the mixture *via* syringe and the reaction mixture was degassed by four freeze-pump-thaw cycles. Finally, 4.63 mg of PMDETA was added to the mixture and stirred in a thermostatic oil bath at 65 °C for 20 h under N_2 atmosphere. After that different concentration of cloisite 93A [DST-24 (0%), DST-25 (1%), DST-27 (2%), and DST-28 (3 wt.%)] dissolved in 3 mL of THF and added into the above mixture and further stirred at 60 °C for 4 h. After 24 h, the polymer functionalization reaction was terminated by pouring the mixture in to 150 mL of hexane. The resulting precipitate was filtered, redispersed in 100 mL of THF and again precipitated to remove the unreacted monomer and Cu(II)/PMDETA complex. The procedures were repeated several times before analyzing the molecular weight by GPC. A pale gray solid was obtained after vacuum drying for 30 h (see Scheme 2). All the experimental data are depicted as the mean of two or three individual experiments. Deviations from mean differences are presented as mean ± SD. The Cells were treated with different concentrations (0, 25, 50, 75, 100, 125 and 150 µg) for 24hrs.

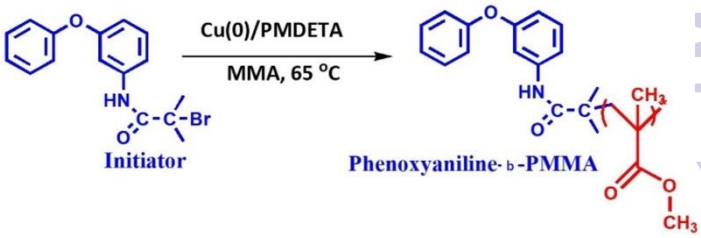

Scheme 2. Synthesis of phenoxyaniline-b-PMMA through SET-LRP.

2.7. Statistical analysis

The cytotoxic effects of DST 24 on A549 cells were determined using the MTT assay. The cells were treated with different concentrations (0, 25, 50, 75, 100, 125 and 150 µg) for 24hrs. The 50% of inhibition was observed at a concentration of 50 µg/mL, (p value: 0.0215), which was taken as the IC-50 value for further experiments. Data are presented as a means ± SD (n=3). *Significant compared with the control-blank group, $p < 0.001$.

For the cytotoxic effect of DST-28 on the prostate cancer cell line, cells were treated with different concentrations (10, 20, 40, 80, 100, and 120µg/mL) for 24hrs. 50% of inhibition was observed at a 40 µg/mL (p-value: 0.0037) concentration, which was taken as the inhibitory concentration (IC-50) dose value and fixed for further experiments. *Signifies statistical significance between control and treatment groups at the $p < 0.05$ level using Student's–Newman–Keuls test.

3 Results and Discussion

3.1. Structural identifications by FT-IR and X-RD

The FTIR spectra for phenoxyaniline initiator (PA), DST-24 , DST-25, DST-27 and DST-28 samples were recorded in the range of 4000-500 cm^{-1} as shown in Fig. 1(a). In the initiator spectrum, the stretching band at 3334 cm^{-1} assigned for N-H stretching vibration is indicating the existence of amine group in the initiator. The presence of aromatic amine group is also confirmed a peak at 1272 cm^{-1} (C-N stretching). Further, the cyclic alkene is observed at the peak of 1657 cm^{-1} (C=C stretching), notable peak at 687 cm^{-1} is attributed to the C-Br stretching vibration and it shows the

presence of halide anion in the initiator, which confirmed the existence of phenoxyaniline in the PA sample. In DST-24, DST-25, DST-27 and DST-28 composite samples has predominant peaks at 3389 cm^{-1}, which indicates the existence of N-H stretching vibration. The band at 1726 cm^{-1} is occurred due to C=O (stretching) stretching vibration band of PMMA and the peaks between 740 and 1300 cm^{-1} have become broad owing to C-O-C band stretching mode of ester moiety from PMMA.[12]

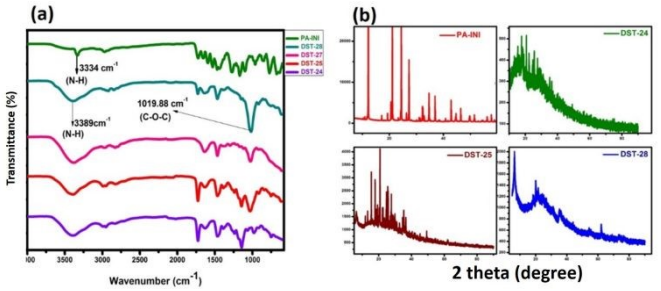

Fig. 1 FT-IR spectra of (a) Phenoxyaniline initiator (PA-INI) and different weight percentages of polymer nanocomposites *via* SET-LRP [DST-24: phenoxyaniline-b-PMMA, without clay, DST-25: 1% clay contained phenoxyaniline-b-PMMA, DST-27: 2% clay contained phenoxyaniline-b-PMMA, DST-28: 3% clay contained phenoxyaniline-b-PMMA] and (b) XRD pattern of Phenoxyaniline initiator and their composites [DST-24, DST-25 and DST-28].

Comparing to the PA initiator, the N-H stretching vibration band is shifted from 3334 to 3389 cm^{-1} in all DST-24, DST-25, DST-27 and DST-28. The vibrational peaks at 1386 cm^{-1} and 748 cm^{-1} could be attributed to the α-methyl group vibrations and the peak at 1468 cm^{-1} can be assigned as the C–H bending vibration of the $–CH_3$ group in PMMA.[13] The peak at 1636 cm^{-1} assigned for C=C (stretching cyclic alkene) band of PMMA. Overall, the synthesized polymer units and initiator functional groups are confirmed by FT-IR technique. Further, XRD analysis was carried to out to investigate the crystalline and phase formation of the synthesized materials. The Fig. 1(b) shows the X-ray diffraction peak at 21.81˚and 63.87˚ (JCPDS No: 04-0783) corresponding to the diffraction planes of (100) and (220), respectively attributing to the existence of phenoxyaniline in the PMMA composite. Fig 1(b) shows the X-ray pattern of phenoxyaniline-based initiator, which shows the peaks at 2Θ: 18.71˚, 20.61˚, 20.91˚, 25.93˚, 29.96˚, 31.02˚, 31.43˚, 32.27 and 41.689˚ corresponding to the diffraction planes of (100), (100), (100), (100), (110), (110), (110), (110), and (200) respectively. The narrow peaks of the XRD patterns clearly confirm their improved crystalline properties. The narrow peak at 20.61˚ is corresponding to a highly crystalline nature of the system, which can be attributed to the presence of halide groups, which is also confirmed by SEM images as shown in Fig. 4. Interestingly, while preparing the PA sample, many white colour crystals were formed in the Petridis as shown in Fig. 4c. Notably, after polymerization, the composite has become amorphous nature for all the samples (DST-24, DST-25 and DST-28) due to incorporation of cloisite at different weight percentages. This can be due to the destruction of the ordered arrangements of the methacrylate in the composite. This emerged amorphous phase can cause a reduction in the energy barrier of polymer chain segmental motion. Further, the obtained XRD pattern clearly show that the crystallinity of the blends is decreased after it is blended with PMMA and it becomes more amorphous in nature, which eventually enhances a greater ionic diffusion and causes more ionic conductivity, hence it becomes viable to inhibit the cancer cells.

3.2 Raman spectroscopy study

The information about the intra and inter molecular mechanism of interaction between phenoxyaniline and PMMA were investigated by Raman spectroscopy using 532 nm laser in the spectral region 50-3500 cm^{-1}.

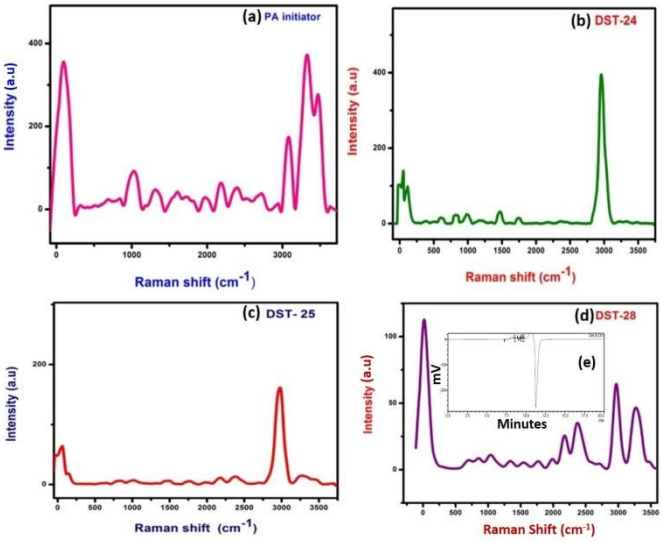

Fig. 2 Raman spectra of (a) Phenoxyaniline initiator, (b) DST-24 (phenoxyaniline-b-PMMA, without clay), (c) DST-25 (1% clay contained phenoxyaniline-b-PMMA) and (d) DST-28 (3% clay contained phenoxyaniline-b-PMMA) and (e) GPC of DST-28 (3% clay contained phenoxyaniline-b-PMMA).

The methylene group (CH_2 at 838 cm^{-1}), which present in the PMMA and the CH_3 groups at 980 cm^{-1} that attached to backbone of carbon and the single oxygen atoms are denoted as α-methyl and the ester methyl and the carbonyl (C-O at 1743 cm^{-1}) group are found to be attached with carbon backbone respectively.[14] However, some of the Raman modes are found to be very weak in their respective region. For example, C-C-O symmetric stretching mode at 608 cm^{-1}, carbonyl group at 1743 cm^{-1} and C-O-CH_3 at 810 cm^{-1} in all the three composite samples are given in Fig 2 (b-d). Notably, the Raman shift is increased with increasing nanoclay contents in the PMMA matrixes. Fig. 2a shows the spectrum of phenoxyaniline based initiator. The spectrum, clearly reveals the functional group at 1010 cm^{-1} (C-O-C) and sharp peak N-H at 3313 cm^{-1}, which are confirmed the formation of phenoxyaniline structure. The specially prepared composition with the highest percentage of clay, containing phenoxy-b-PMMA with M_n: 3112, M_w: 3595 and PDI: 1.15 as shown in Fig. 2e, which confirm the success of controlled radical polymerization.

3.3. UV-*vis* spectroscopy, particles measurements and thermal study

The DSC experiment was carried out in the temperature ranges from -50 °C to 250 °C with the heating rate of 10° C/min under nitrogen atmosphere. The polymer composite sample of 12 mg was encapsulated in aluminum pan. DSC plot of polymer containing 3% filler shows the sharp exothermic peak, which indicates the transition from semi-crystalline to amorphous phase. DSC results showed that the T_g of phenoxyaniline-b-PMMA (DST-28) is found to be ~115°C (see Fig. 3a). There decrease in Tg could be due to the addition of cloisite 93 A, which increases the segmental motion of the polymer unit.

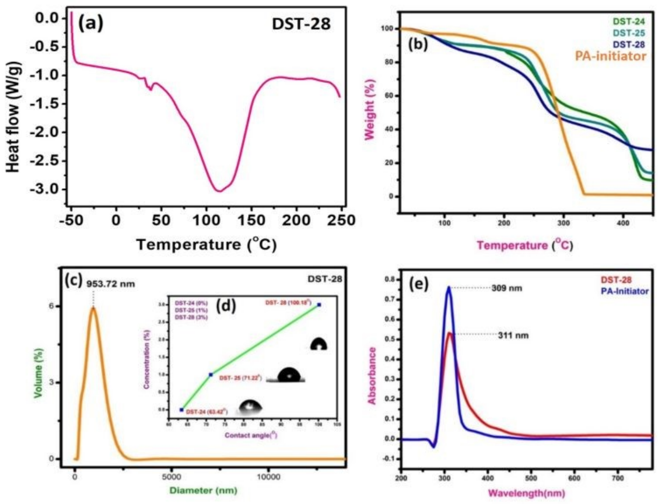

Fig. 3 (a) Differential scanning calorimetry (DSC) thermogram of DST-28 (enthalpy: 599.51 J/g, 10 °C/min.), (b) Thermo-gravimetric analysis (TGA) of various percentages of polymer composites; DST-24 (phenoxyaniline-b-PMMA, without clay), DST-25 (1% clay contained phenoxyaniline-b-PMMA), DST-28 (3% clay contained phenoxyaniline-b-PMMA) and phenoxyaniline initiator, (c) Particles size analysis of DST-28 (3% clay contained phenoxyaniline-b-PMMA), (d) Contact angle measurements of different percentages of composites: DST-24 (phenoxyaniline-b-PMMA, without clay), DST-25 (1% clay contained phenoxyaniline-b-PMMA), DST-28 (3% clay contained phenoxyaniline-b-PMMA) and (e) UV-*vis* spectra of macroinitiator with highest percentage of composite (DST-28 with 3% clay).

The pure PMMA has a melting temperature of around 160 °C, but phenoxyaniline blocked PMMA tend to decrease their T_g. The softening temperature is found to be decreasing when the symmetrical structure is changed into asymmetrical structure, which implies that there is a reduction in the crystallinity of the polymer composite. There are three main stages of degradation of phenoxyaniline-b-PMMA. Moreover, the first stage is complex for all the samples except pure PMMA. The polymer content on the phenoxyaniline is determined by means of TGA, which confirms the growth of polymer on the surface through various weight loss measurements. The TGA trace for phenoxyaniline-b-PMMA shows a significant shift in the weight loss towards higher temperature with a thermal stabilization of 30 °C, which is higher than that for a neat PMMA. The enhanced thermal stability observed for phenoxyaniline-b-PMMA composites are influenced by the interaction between the polymer and cloisite, as evident by thermogram (Fig. 3b). In the TGA curve of initiator distinguishes two weight loss stages during the thermal decomposition of the sample. The first stage shows that the decomposition or loss of the absorbed and combined water and the evaporation of residual solvent. In the second stage, after 330 to 450 °C, it shows some of decomposition of the sample. While increasing the filler content in the polymer network, the thermal stability is also increased. The sample DST-28 with 3 wt% cloisite 93 A shows the drastic weight loss, which may be attributed to the melting of the polymer. The prepared polymer composites stable up to 450 °C. For the contact angle measurements by the sessile drop method, Holmarc, HOIIDCAM-01B, Contact Angle Meter, India video-camera system equipped with the computer software was used. The contact angles of probe liquid were measured at 20±1° in a closed chamber. The advancing contact angles of water of 100 μL volume was measured after settling droplets on the glass surface. Then after sucking of one-third from the droplet into the syringe, the receding contact angle was measured. Fig 3(d) shows (DST-24, CA: 63°) good hydrophilic nature, however, while increasing the concentration of cloisite 93A onto polymer mixture (DST-25:CA:80° and DST-28:CA:121°), it become hydrophobic nature, which means that the polymer composite have better wettability. Moreover, we also analyzed the particles size of the polymer composite, which show the average particle size is around 953 nm by particle size analyser (see Fig 3c). The UV visible spectra of the initiator and DST-28 have been analyzed ranging from 300 to 600 nm. In Fig 3(e) the maximum absorption was obtained at 300nm, which is due to the saturated aliphatic polymer with a carbonyl group as a chromophore. The most typical absorption band for carbonyl compounds is that of the n-π* transition. This transition usually requires the smallest energy so that the band has the largest wavelength in the region at 280-300 nm. Interestingly, there is no evidence of absorption in the range of 400 to 800 nm for both the samples. In Fig. 3(e), the initiator was used to polymerize the MMA monomer where the band is observed at 300 nm and found that it is slightly broad up to 450 nm due to the well-controlled polymerization. This n-π* transition is "forbidden" in symmetry terms and, therefore, the intensity is low after polymerization. The observed low intensity absorption band at 320 nm may be due to the n-σ* transition occurring in carbonyl groups present in PMMA molecules.

3.4 Morphological study by SEM

Phenoxyaniline was brominated using bromoisobutryl bromide in dichlromethane solvent medium, after reaction, the mixture was washed with diethyl ether for several times and kept it in room temperature. After 2 days, we observed that a white colour crystals were formed after complete evaporation of organic solvent, which showed in Fig 4c. Same sample was analyzed by SEM, which showed layered by layered crystals with average width size ~100 nm (see Fig. 4a-b). It has already been recommended that the morphology of layered crystals of PA macroinitiator strongly depended on the agreeing solvent evaporation rate. A low solvent evaporation typically leads to higher formation of crystals.

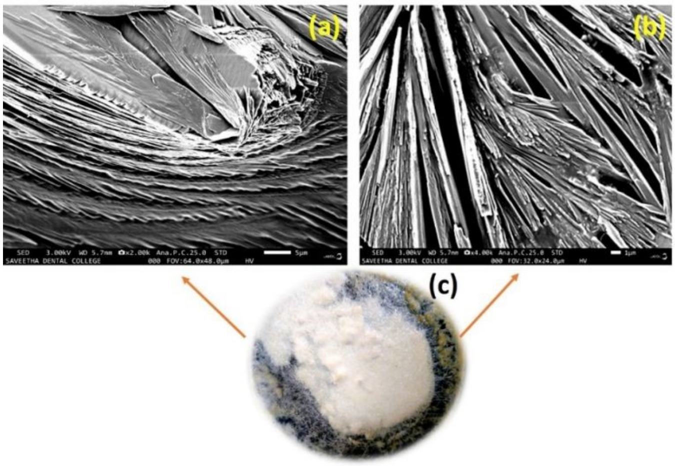

Fig. 4. Scanning electron microscopy (SEM) images of Phenoxyaniline initiator after complete removal of organic solvent with layered by layer white crystals (a) 5 µm size, (b) 1 µm size and (c) photographical image of white crystals based phenoxyaniline initiator.

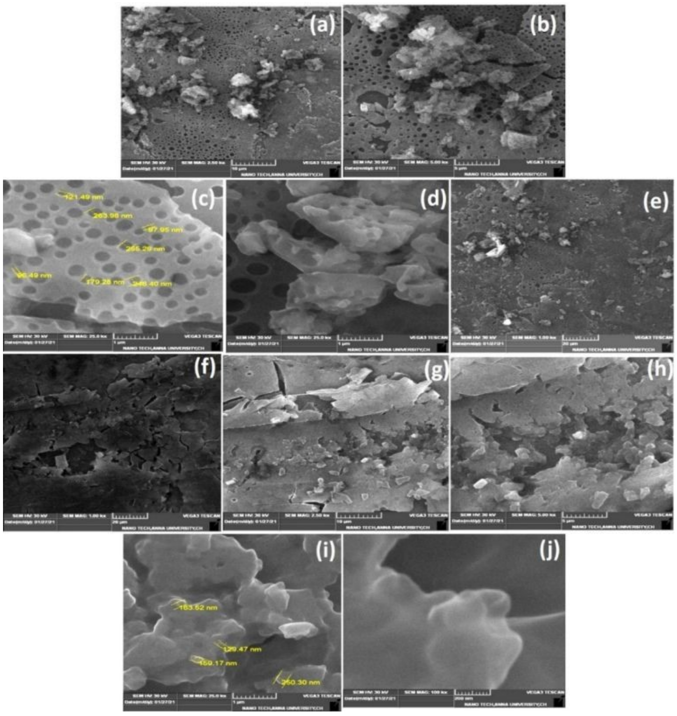

Fig. 5 SEM images of Phenoxyaniline-b-PMMA without clay content from (a-e): (a) Porous structure at 10 µm, (b) 5 µm size, (c-d) 1 µm with an average pore size diameter of 172 nm size and (e) 20 µm size. (f-j) Phenoxyaniline-b-PMMA with 3% clay content: (f) 20 µm size, (g) 10 µm size, (h) 5 µm size, (i) 1 µm with clay flakes approximately 170 nm in diameter, and (j) 200 nm size.

The prepared initiator and polymer composites samples were investigated through SEM to evaluate the surface changes with and without the filler. Further, the macroinitiator was utilized to polymerize the MMA monomer to afford porous polymer composites. In Fig 5(a), the SEM micrograph of DST-24 clearly shows the porous like structure. A quite homogeneous pores distribution was fabricated without the filler (cloisite) with average pore size 97 nm (see Fig. 5a-e). Subsequently, in the micrograph of DST-28 containing 3% of cloisite 93 A, it is observed that there are less macropores due to higher percentage of clay content in the PMMA network and some of the cell windows are closed in the pore walls. The polymer composites were also subjected to XRD, which clearly agreed the formation of amorphous and crystals. SEM images also clearly suggested that the incorporation of clay content in the polymer matrixes led to intercalated well and the higher percentages of clay led to the agglomerated structure as shown in Fig 5(f-j) and all the clay layers were found to be with an average size of 159-163 nm, thus could not get homogeneously dispersed PMMA matrix.[15]

3.5. Anticancer activities of Phenoxyaniline-b-PMMA (without nanoclay) against lung cancer (A549)

Based on the MTT assay, it can be inferred that there was a significant cytotoxic activity of the DST-24 against lung cancer cell lines (A549). It was identified that the inhibitory concentration for this DST-24 is 50 µg/mL.

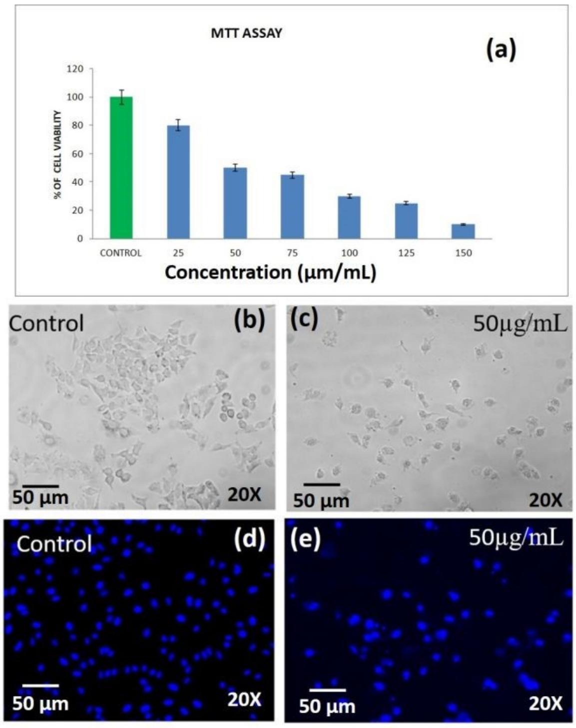

DAPHI stain

Fig. 6. (a) MTT assay of DST-24 on A549 cells, (b, c) morphological changes in lung cancer cell line upon without and with treatment of DST-24 at 50 µg/mL for 24 hrs by phase contrast microscope at 20x magnification (scale bar 50µm), (d, e) Induction of apoptosis in DST-24 treated lung cancer cell line and nuclei were stained with DAPI staining and observed under a fluorescence microscope (20x magnification, scale bar 50µm).

Table 1. Percentages of cell viability against A-549 cell lines.

S. N	IC-50, Cell viability test against lung cancer cell lines (A-549)-DST 24							
1.	Concentration	Control	25	50	75	100	125	150
	Percentage of cell viability	100	80	50	45	30	25	10

The cell morphology showed comparison of the differences in cell morphology of the control and the cell morphology of the cell lines treated with the DST-24. It was observed that the number of cells decreased after treatment and the cells exhibited cell shrinkage and cytoplasmic membrane blebbing (see Fig. 6). Previous studies also analyzed the changes in cellular morphology of the cancer cell line. Their studies also confirmed similar cellular changes with increased free-floating cells.[16,17] The DAPI staining apoptosis test results suggest that there was condensation of chromatin and nuclear fragmentation which occurred owing to the process of apoptosis.[18] These changes were observed under fluorescent microscopy. These results obtained in our study are supported by the previous similar studies done, where the most anti-cancer effects are based on the apoptotic activity of the chemotherapeutic agents.[19,20] However, the future in-vivo studies need to be performed for better understanding and usage of phenoxyaniline-b-PMMA as a cytotoxic agent. Also, IC-50 doses and Cell viability against A-549 cell lines were shown in Table 1.

3.6. Anticancer activities of DST-28 against prostate adenocarcinoma cancer cell line (PC-3)

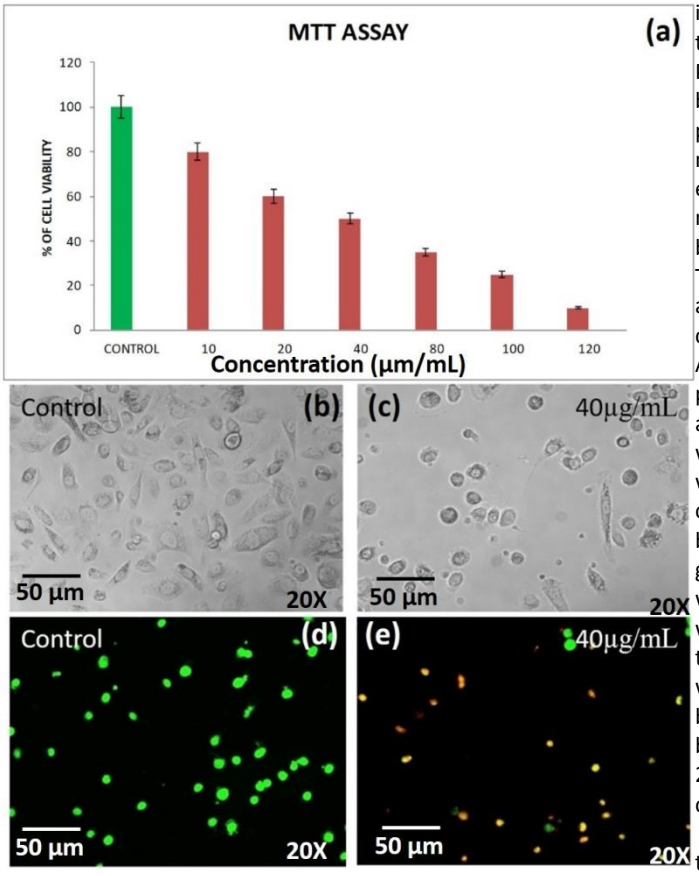

Fig. 7. (a) cytotoxic effect of DST-28 (with nanoclay) against the prostate cancer cell line, (b,c) Phase-contrast microscopic images of DST-28 compound on cell morphological changes in the prostate cancer cell line (20x magnification, 50µm scale bar), (d, e) The PC-3 cells treated with DST 28 at 40 µg/mL concentration and viewed under fluorescence microscope at 20x magnification (scale bar 50µm).

Table 2. Percentages of cell viability against PC-3 cell lines.

S. N	IC-50, Cell viability test against prostate cancer cell lines (PC-3)-DST 28							
1.	Concentration	Control	10	20	40	80	100	120
	Percentage of cell viability	100	80	50	45	30	25	10

Apoptosis is a programmed cell death that serves as an important mechanism for tissue homeostasis and cell eradication and by inhibiting metabolic activation, boosting detoxification, or offering alternate targets for electrophonic metabolites, these substances aid in the prevention of carcinogenesis.[22,23] The cytotoxic effect of DST-28 extract on cell lines was calculated by micro-culture tetrazolium assay (MTT). The multiple concentration of DST-28 was used and IC50 doses were calculated (see Table 2). The MTT assay results showed that the dose dependent (10-120µg/mL) cell growth inhibition was observed in DST-28 treated against PC-3 cells. The IC-50 dose was observed at 40µg/mL. Since DST 28 has better cytotoxic activity against PC-3 cells, it was used for further investigation. Morphological investigation of apoptosis revealed that DST-28 at a concentration of 40µg/mL induced cell death in the PC-3 cell line by apoptosis. Phenotypically apoptosis is characterized by cell shrinkage, DNA fragmentation, chromatin condensation, plasma mem-brane blebbing, and collapse of the cell into small membranes. The phase-contrast image shows that DST-28 has exhibited the morphological changes such as reduction in the number of cells, cell shrinkage, and cytoplasmic membrane blebbing in the treated cells when compared with untreated cells. The DST-28 exhibited exceptional antioxidant activity in all antioxidant tests and significantly reduced lipid peroxidation at a concentration of 50 g/mL, according to prior research report.[24] AO\EtBr (acridine orange and ethidium bromide) dual staining was performed to determine if exposure to DST-28 causes cell death by apoptosis in PC-3 cell lines. In the AO/EtBr staining, the viable cells will possess a uniform bright green nucleus. The early apoptotic cell will have bright orange areas of condensed or fragmented chromatin in the nucleus. Late apoptotic cells will have a uniform bright red nucleus. It was found that un-treated cells were mostly green with an intact nucleus. AO\EtBr analysis showed that DST-28 was cytotoxic towards PC-3 cells through apoptosis when treated with IC50 con-centration (40 µg/mL). In the AO\EtBr analysis, cells treated with IC 50 value of DST-28 showed a red color nucleus, which further confirmed the induction of late apoptosis in PC-3 cells by DST-28 (see Fig. 7). This finding was characterized by membrane blebbing and nuclear shrinkage. The above data indicate that DST-28 inhibits cell proliferation and induces apoptosis in prostate cancer cells.

Conservative precision medicine for cancer treatment as one of the most promising methods to undertake various cancers by developing the effective drugs. In this study, we developed a novel polymer nanocomposite as an anti-cancer drug molecules to treat the lung and prostate cancers. Phase contrast microscopy was used to analyses the changes in cell morphology of the lung cancer cell lines when treated with DST-24 (without nanoclay). The changes in cell morphology among the lung cancer cell lines treated with 50 µg/mL concentration DST-24 was compared with the control group for 24 hours. The results suggest that the treated cells showed

characteristic changes similar to that of apoptotic cells- shrinkage of cells with reduced cell density. Some cells also showed other changes much like that of apoptotic cells like cell roundening and loss of contact with adjacent cells. Some cells detached themselves from the base of the plates. DAPI staining was used to analyses the induction of apoptosis among the lung cancer cell lines treated with DST 24 (50 µg/mL) after 24 hours. Fluorescence microscopy was used to check the pro-apoptotic effect post staining. The results suggested that the cancer cell lines treated with the leaf extract showed condensation of chromatin along with nuclear fragmentation. These changes are suggestive of characteristic apoptotic activity when compared to the control group which had round nuclei. MTT assay was used to assess the cytotoxic potential of phenoxyaniline-b-PMMA (DST-24) on the lung cancer cell lines. Various concentrations of the extract (25-150 µg/mL) were tested against the lung cancer cell line for 24 hours. The results of the assay suggested that there was a significant decrease in the viability of lung cancer cell lines (A-549) when treated with DST-24, when compared to the control for 24 hours. The viability of the cells was gradually decreased with increasing concentration of the DST-24. It was observed that 50% growth inhibition occurred at a concentration of 50 µg/mL. Thus, the IC-50 dose considered for further experiments was about 50 µg/mL (see Fig 6a). Further, we studied the anti-cancer activity of DST-28 against prostate adenocarcinoma cancer cell line (PC-3). It showed prominent results on prostate cancer cell line. DST-28 has excellent cytotoxic effect against PC-3 cell lines, further it was investigated on their cell morphological behaviors under fluorescence and contract mi-croscopy and it has cell shrinkage, DNA fragmentation, chromatin condensation, plasma membrane blebbing, and collapse of the cell into small membranes. Cloisite 93 A nanoclay, with its specific chemical composition, surface-area-to-volume ratio, charge and size, possesses high surface properties that can interfere with the function of cancer cells, disrupting cellular processes and inhibiting cell division in cancer cells. Additionally, nanoclays can adsorb biomolecular, including proteins onto their surfaces. This can alter cellular microenvironment and affect the signalling pathways that cancer cells rely on for growth and survival. Moreover, nanoclays can release ions such as magnesium or iron, when exposed to the intracellular environment of cancer cells. These ions can disrupt cellular processes and inhibit the cancer cell growth. Nanoclays can also generate reactive oxygen species (ROS) when exposed to cellular environments. Elevated ROS levels can lead to oxidative stress in cancers cells, causing damages to cellular components and ultimately inhibiting cell proliferation. However, it is important to note that nanoclays are generally considered biocompatible and do not inherently harm or damage living cells. Findinds from invitro studies may not fully represents the complexity of interaction that occurs in living cells, therefor, its essential to conducts in-vivo studies in animal models to assess the overall toxicity and safety of nanoclays in a more physiological context. The use of a phenoxyaniline-based macroinitiator for producing these composites is novel approach. Adding different weight percentages of Cloisites 93-A to the polymer matrixes facilitates to enhance their biochemical properties and crucial applications, where the biocompatibility and bioactivity are essential, such as in medical or pharmaceuticals formulations. The excellent anticancer properties, including cancer cell apoptosis induction, hold significant importance in medicine and oncology. Furthermore, utilizing the nanoclays for cancer treatment owing to their complete water solubility and its ability to form cationic complexes with drugs through electrostatic interactions is an innovative approach. Experimental conditions are carefully controlled to ensure the accurate and reproducible results, including temperature, pressure, reactant concentration and specific equipment for characterization and analysis process. Introducing the impact of nanoclay on phenoxy-based PMMA composites for anticancer treatment could be a new and pioneering development in the field. Further, we also confirmed their structural identifications by FT-IR, Raman, UV-vis and XRD. Interestingly, layer by layer crystals were formed and confirmed by SEM. In conclusion, to the best of our knowledge, this is the first time to employ such kind of blocked polymer nanocomposite through SET-LRP towards the cancer treatment against PC-3 and A-549 cell lines.

4. Conclusions

We have successfully synthesized the phenoxyaniline-b-PMMA *via* controlled radical polymerization (SET-LRP) using phenoxyaniline based macroinitiator and characterized by various analytical techniques. Here, we showed that there were differential cellular responses in both prostate and lung cancer cell lines. Polymer containing cationic nanoclay was favoured to inhibit the cancer cell proliferations through electrostatic interaction. It showed excellent cytotoxic effect in both cancer cell lines by using MTT assay and their bright green nucleus (viable cells), bright orange nucleus (early apoptotic cells- fragmented chromatin nucleus) and bright red nucleus (late apoptotic cells) were successfully identified by Fluorescence microscopy. The number of cells was decreased after treatment and the cells exhibited as cell shrinkage and cytoplasmic membrane blebbing. As a result, our study suggested that the prepared polymeric nanocomposites could be affective alternative material in precision anti-cancer medicine. The analysis of the dynamics of individual interactions within cells is under progress.

Acknowledgements

This research was supported by the National Research Foundation of Korea (NRF) (Grant No: 2020R1A6A1A03044512), Korea Institute of Planning and Evaluation for Technology in Food, Agriculture and Forestry (IPET) funded by Ministry of Agriculture, Food and Rural Affairs (MAFRA)(321027-5). The author (Dr. A. Murali) thankful to the Department of Science and Technology (DST), Govt. of India, grant no: DST/INSPIRE/04/2018/001762 for DST Inspire Faculty.

Author Contributions: Writing original draft preparation, Conceptualization and methodology: S.P, A.M, and SM; formal analysis: A.L, S.S, and DM; funding, review and editing: RR, SSH and A.M. All authors have read and agreed to the published version of the manuscript.

References

1 J. Kim, Y. M. Lee, Y. Kang, W. J. Kim, Tumor-homing, size-tunable clustered nanoparticles for anticancer thera-peutics, *ACS Nano*, 2014, **8**, 9358-9367.

2 Y. B. Liu, X. Gao, D. Deeb, C. Brigolin, Y. Zhang, J. Shaw, K. Pindolia, S. C. Gautam, Ubiqui-tin-proteasomal degradation of antiapoptotic survivin facilitates induction of apoptosis in

prostate cancer cells by pristimerin, *Int. J. Oncol,* 2014**, 45**, 1735-1741.

3 Y. Kumar, N. K. Singh, V. D. I. Singh, Ali, R. K. Tiwari, A. Kumar, D. S. Pandey, DNA/Protein binding and anti-cancer activity of Zn (II) complexes based on azo-Schiff base ligands, *Inorganica Chim. Acta,* 2022, **538**, 120963.

4 F. Hosseini, F. Hosseini, S. M. Jafari, Taheri, A. Bentonite nanoclay-based drug-delivery systems for treating melanoma. *Clay Miner,* 2018, **53**, 53–63.

5 H. A. Patel, R. S. Somani, H. C. Bajaj, R. V. Jasra, Nanoclays for polymer nanocomposites, paints, inks, greases and cosmetics formulations, drug delivery vehicle and waste water treatment, *Bull. Mater. Sci,* 2006**, 29,** 133–145.

6 K. Sparnacci, M. Laus, L. Tondelli, L. Magnani, C. Bernardi, Core–shell microspheres by dispersion polymer-ization as drug delivery systems, *Macromol Chem Phys,* 2002, **203**, 1364- 1369.

7 H. P. Zobel, J. Kreuter, D. C. Werner, R. Noe, G. Kumel, A. Zimmer, Cationic Polyhexylcyanoacrylate Nanopar-ticles as Carriers for Antisense Oligonucleotides, *Drug Deliv,* 1997, **7,** 483-493.

8 K. S. V. K. Rao, I. Chung, K. M. Reddy, C. Sik Ha, PMMA-based microgels for controlled release of an anticancer drug, *J. Appl. Polym. Sci,* 2009, **111**, 845-853.

9 C. Geyik, M. Ciftci, B. Demir, B. Guler, A. B. Ozkaya, Z. P. Gumus, F. B. Barlas D. O. Demirkol, H. Coskunol, S. Timur, Y. Yagci, Controlled release of anticancer drug Paclitaxel using nano-structured amphiphilic star-hyperbranched block copolymers, *Polym.Chem*, 2015, **6**, 5470-5477.

10 S. P. 1Akhlaghi, S. Saremi, S. N. Ostad, R.; Dinarvand, Atyabi, F. Discriminated effects of thiolated chi-tosan-coated pMMA paclitaxel-loaded nanoparticles on different normal and cancer cell lines, *Nanomedicine,* 2010, **6**, 689-697.

11 M .F. Cury-Boaventura, C. Pompéia, R. Curi, Comparative toxicity of oleic acid and linoleic acid on Jurkat cells, *Clin. Nutr*, 2004, **23**, 721-732.

12 J. i. Li, R. Hu, H. Zhou, S. Tao, Y. Wang, Nano-SiO2@PMMA-doped composite polymer PVDF-HFP/PMMA/PEO electrolyte for lithium metal batteries, *J. Mater. Sci. Mater. Electron*, 2020, **31**, 2708–2719.

13 C. M. Mathew, K. Kesavan, S. Rajendran, Structural and Electrochemical Analysis of PMMA Based Gel Elec-trolyte Membranes, *Int. J. Electrochem. Sci*, 2015, 1-7.

14 G. Mingming, S. Aman, P. L. Robert, Impact of moderate pump–Stokes chirp on femtosecond coherent anti-Stokes Raman scattering spectra, *J Raman Spectrosc*, 2020, **51**, 115-124.

15 A. Arora, V. Choudhary, D. K. Sharma, Effect of clay content and clay/surfactant on the mechanical, thermal and barrier properties of polystyrene/organoclay nanocomposites, *J. Polym. Res*, 2011, **18**, 843–857.

16 A. Elhussein, I. Tynga, M. A. El-Harith, H. Abrahamse, Photodynamic ability of silver nanoparticles in induc-ing cytotoxic effects in breast and lung cancer cell lines*, Int. J. Nanomedicine,* 2014, **9**, 3771-3780.

17 S. L. Manoto, H. Abrahamse, Effect of a newly synthesized Zn sulfophthalocyanine derivative on cell morphol-ogy, viability, proliferation, and cytotoxicity in a human lung cancer cell line (A549), *Lasers Med. Sci*, 2011, **26,** 523–30.

18 D. Ezhilarasan, V.S. Apoorva, Syzygium cumini extract induced reactive oxygen species-mediated apoptosis in human oral squamous carcinoma cells, *J. Oral Pathol. Med*, 2019, **48**, 115-121.

19 S. Usmani, A. Hussain, A. H. A. Farooqui, M. Arshad, S. Siddiqui, M. Ahmad, S. Wahab, Anti-proliferative Activity of Crude Extract and Fractions Obtained from Digera muricata on HeLa Cell Lines of Human Cervix and A549 Cell Lines of Human Lung. *Phcog J,* 2014, **6,** 32-38.

20 P. Suresh, K. Marimuthu, S. Ranganathan, T. Rajmohan, Optimization of machining parameters in turning of Al-SiC-Gr hybrid metal matrix composites using grey-fuzzy algorithm, *Trans. Nonferrous Met. Soc. China,* 2014, **24,** 2805–2814.

21 A. Sathivel, H. R. B. Raghavendran, P. Srinivasan, T. Devaki, Anti-peroxidative and anti-hyperlipidemic nature of Ulva lactuca crude polysaccharide on D-galactosamine induced hepatitis in rats, *Food Chem. Toxicol,* 2008**, 46,** 3262-3267.

22 L. Govindaraju, P. Neelakantan, J. L. Gutmann, Effect of root canal irrigating solutions on the compressive strength of tricalcium silicate cements, *Clin. Oral Investig.* 2017, 567-571.

23 T. Sathish, S. Karthick, Wear behaviour analysis on aluminium alloy 7050 with reinforced SiC through taguchi approach*, J. Mater. Res. Technol.* 2020, **9,** 3481–3487.

24 H. Krishnaswamy, S. Muthukrishnan, S. Thanikodi, G. Arockiaraj, V. Venkatraman, Investigation of air conditioning temperature variation by modifying the structure of passenger car using computational fluid dynamics, *Therm. Sci.* 2020, 495–498.